Charge control of blockade of Cooper pair tunneling in highly disordered TiN nanowires in an inductive environment

S. E. de Graaf,[1,*] R. Shaikhaidarov,[2,3] T. Lindström,[1] A. Ya. Tzalenchuk,[1,2] and O. V. Astafiev[1,2,3]
[1]*National physical laboratory, Hampton Road, Teddington, TW11 0LW, United Kingdom*
[2]*Royal Holloway, University of London, Egham, TW20 0EX, United Kingdom*
[3]*Moscow Institute of Physics and Technology, Dolgoprudny, Russia*

(Received 29 October 2018; revised manuscript received 13 March 2019; published 10 May 2019)

A central problem in understanding the superconductor-insulator transition in disordered superconductors is that the properties of grains and intergrain medium cannot be independently studied. Here we demonstrate an approach to the study of strongly disordered superconducting films by relying on the stochastic nature of the disorder probed by electrostatic gating in a restricted geometry. Charge tuning and magnetotransport measurements in quasihomogeneous TiN nanowires embedded in a superinductor environment allow us to classify different devices and distinguish between spontaneously formed Coulomb islands (with typical blockade voltage in the mV range) and homogeneous wires showing behavior indicative of coherent quantum phase slips (with significantly smaller blockade voltage).

DOI: 10.1103/PhysRevB.99.205115

I. INTRODUCTION

The superconductor-insulator transition (SIT) in disordered superconducting thin films is gaining increasing attention for its relevance in a range of applications in superconducting and quantum electronics [1–3] and electrical metrology [4]. The SIT occurs as a result of Anderson localization or as Coulomb interaction breaks global phase coherence, the latter often described by the proliferation of quantum phase slips (QPS) forming a normal matrix around spontaneously formed localized regions of superconductivity [5–7]. The disorder [8,9] and magnetic field [10–13] driven SIT have been extensively studied in thin 2D films and more recently nanopatterned devices [4,10,14–17] of highly disordered superconductors such as InO, NbN, NbTiN, and TiN. Nanowires of these materials are of particular interest in the view of their proposed applications in quantum devices and electrical metrology [15,18,19].

While radio-frequency measurements have demonstrated the coherence of QPS in a range of materials [20–24], it remains a significant challenge in DC measurements. To ensure large quantum phase fluctuations it is essential to embed such nanowires in a high impedance environment. The resulting insulating state due to blockade of Cooper-pair tunneling occurs below a critical voltage $V_c = 2\pi E_s/2e$, due to the QPS rate E_s/h. The most straightforward implementation of a high impedance environment, a resistive environment, is generally incompatible with DC currents due to Joule heating [18]. Alternatively, embedding the QPS element in a superinductor [3,6,25,26] ensures the required dynamics [19,27].

In this work we perform magnetotransport studies of TiN nanowires of width 2–3ξ_0, where ξ_0 is the BCS coherence length, embedded in a high impedance inductive environment. The presented devices were selected from a larger set to highlight distinctively different regimes observed. All devices were designed to be identical and made from the same superconducting film. From the dependence of the voltage blockade on magnetic field and electrostatic gate we find that nanowires of similar dimensions fall into significantly different regimes. We focus on three different devices: Larger blockade voltages (in the mV range) can be attributed to single-electron transistors (SETs) with a behavior consistent with the grain size of the film. In contrast, wires with significantly smaller V_c show a qualitatively different behavior; the gate modulation of the blockade is very weak, and V_c is suppressed at large magnetic fields. We discuss this latter scenario in terms of QPS in a homogeneous wire. A third device shows an intermediate regime, supporting these conclusions. Our results provide additional insight into recent experiments in somewhat wider TiN nanowires closer to the SIT [14] and shed further light on the nature of the SIT in nanopatterned TiN films, enabled by charge control.

II. EXPERIMENT

The devices were made from the same TiN thin film deposited using plasma-assisted atomic-layer deposition (ALD) on a high resistivity Si(100) substrate using the same method and equipment as described in Ref. [28]. Further fabrication and measurement details are outlined in the Supplemental Material [29]. The device design is shown in Fig. 1(a). Figure 1(b) shows the overall measurement circuit and Fig. 1(c) illustrates the different regimes found in the devices presented. We note that this is a very simplified picture useful for the classification of regimes, the real microstructure is likely much more complicated.

*sdg@npl.co.uk

 ©2019 American Physical Society

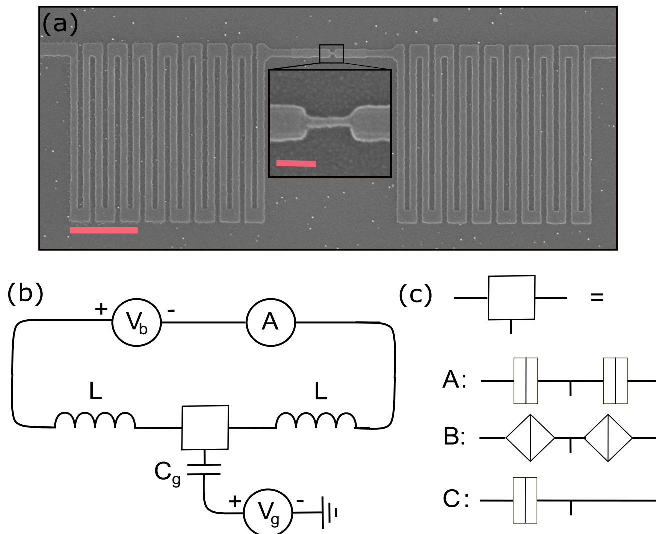

FIG. 1. (a) Scanning electron micrograph of a typical device. Scale bars are 1 μm and 100 nm for the meanders and the closeup of the constriction, respectively. (b) Equivalent circuit with the various device regimes explored is represented by a square and clarified in (c) with a simplified schematic of each of the presented devices A–C.

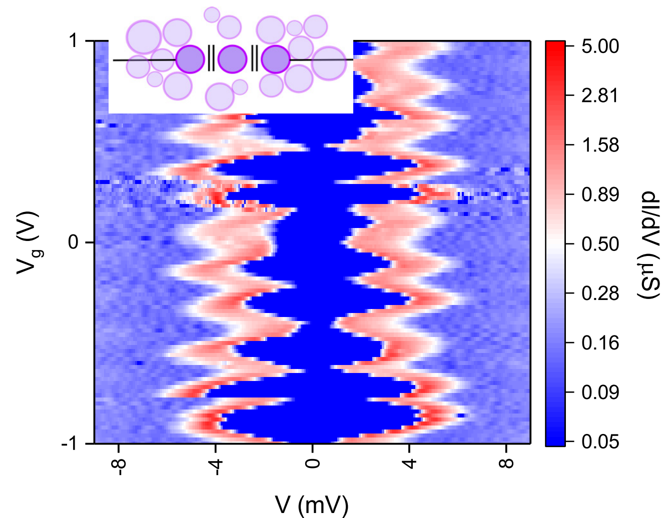

FIG. 2. Conductance of device A versus back-gate voltage, measured in the superconducting state at 10 mK and 600 mT (perpendicular field). The behavior remains the same above the critical field when superconductivity is suppressed (see Supplemental Material [29]). The inset shows a very simplified sketch of a possible microscopic device geometry; circles represent grains.

Each nanowire is approximately 20–30 nm wide and 100 nm long and is symmetrically embedded in a wider meandering nanowire of width 100 nm and length ≈50 μm ($N_\square =$ 480 squares on each side, respectively). The footprint of each meandered superinductor is approximately 3×3 μm^2, giving it a self-capacitance $C_m \approx 0.2$ fF. From the measured normal state resistance we find a sheet resistance of $R_\square =$ 3.0 kΩ which translates to a sheet kinetic inductance $L_{k,\square} = \hbar R_\square/\pi\Delta = 4.4$ nH, using the BCS gap $\Delta = 1.76 k_B T_c$ and measured critical temperature $T_c = 1.0$ K. This results in an impedance of the circuit in the superconducting state, as seen by the nanowire, of $Z_m = 2\sqrt{N_\square L_{k,\square}/C_m} \approx 200$ kΩ, larger than the superconducting resistance quantum $R_{2q} = h/4e^2 \approx$ 6.5 kΩ. In the normal state each meander has a resistance of $R_m = 1.45$ MΩ $\gg R_q = h/e^2$.

III. RESULTS

A. Material properties

From isotherms of $R(B)$, we find the diffusion constant $D = 3.6 \times 10^{-5}$ m^2 s^{-1} and a coherence length in the dirty limit $\xi_0(T = 0) \approx 12$ nm (see Supplemental Material for details), in good agreement with previous findings in similar films [30]. The disorder induced SIT and the competition between superconductivity and Coulomb repulsion in these films [28] results in a reduction of T_c as the film thickness is reduced. In contrast to distinctly granular films the observed superconducting transition remains sharp (for our film $T_c =$ 1.0 K and $\delta T_c = 0.4$ K), a signature of average homogeneous disorder. Such a superconductor can be regarded as granular on length scales smaller than the critical dimension for supporting superconductivity in a single isolated grain [5] $b < b_{\rm crit} = (\nu\Delta)^{-1/3} \approx 8$ nm, where b^3 is the grain volume and $\nu = (e^2 D R_\square d)^{-1} \approx 13$ eV^{-1} nm^{-3} is the density of states (DOS) at the Fermi level. For a grain level spacing $\delta > \Delta$ a single grain is too small to support superconductivity, and the observed superconductivity is a result of intergrain coherence. Nevertheless, superconducting fluctuations will suppress the DOS near the Fermi level due to electron-phonon coupling [5]. For the typical grain size $b \approx 4$ nm [28] we obtain an average grain level spacing $\delta/k_B = (\nu b^3 k_B)^{-1} \sim 14$ K $\gg \Delta$.

B. Large blockade devices

The nature of these devices is most clearly elucidated from the conductance in response to a substrate back-gate voltage, shown for one device in Fig. 2 (device A). The gate dielectric is provided by the 300 μm Si substrate. A gap modulation with a period of ∼180 mV is observed. This is the typical behavior of a (superconducting) SET. The amplitude of oscillations in $V_c \sim 4$ mV could not be due to QPS as this would require a pair of pointlike QPS junctions, each with V_c exceeding Δ/e by one order of magnitude. For the device in Fig. 2 we find the total capacitance $C_\Sigma = e/\max(V_c(V_g)) =$ 40 aF, a charging energy $E_c/k_B = e^2/2C_\Sigma k_B = 23$ K, and a gate capacitance to the effective island $C_g = e/\delta V_g \approx 0.9$ aF, consistent with that of an island of area ≈20 nm^2 in our back-gate geometry. This size agrees well with the observed grain size in these films [28], and it follows that the tunnel junction capacitance $C_J \sim 20$ aF is given by an insulating gap between grains of 1–2 nm ($\varepsilon_r = 110$ [31,32]). Similar values for C_g and C_Σ were found for all devices showing a larger blockade voltage $V_c \sim$ 1–5 mV $\gg \Delta/e$ (we have characterized three such devices).

C. Small blockade

We now turn to a device (B) with strongly connected grains (as will become apparent in the following discussion),

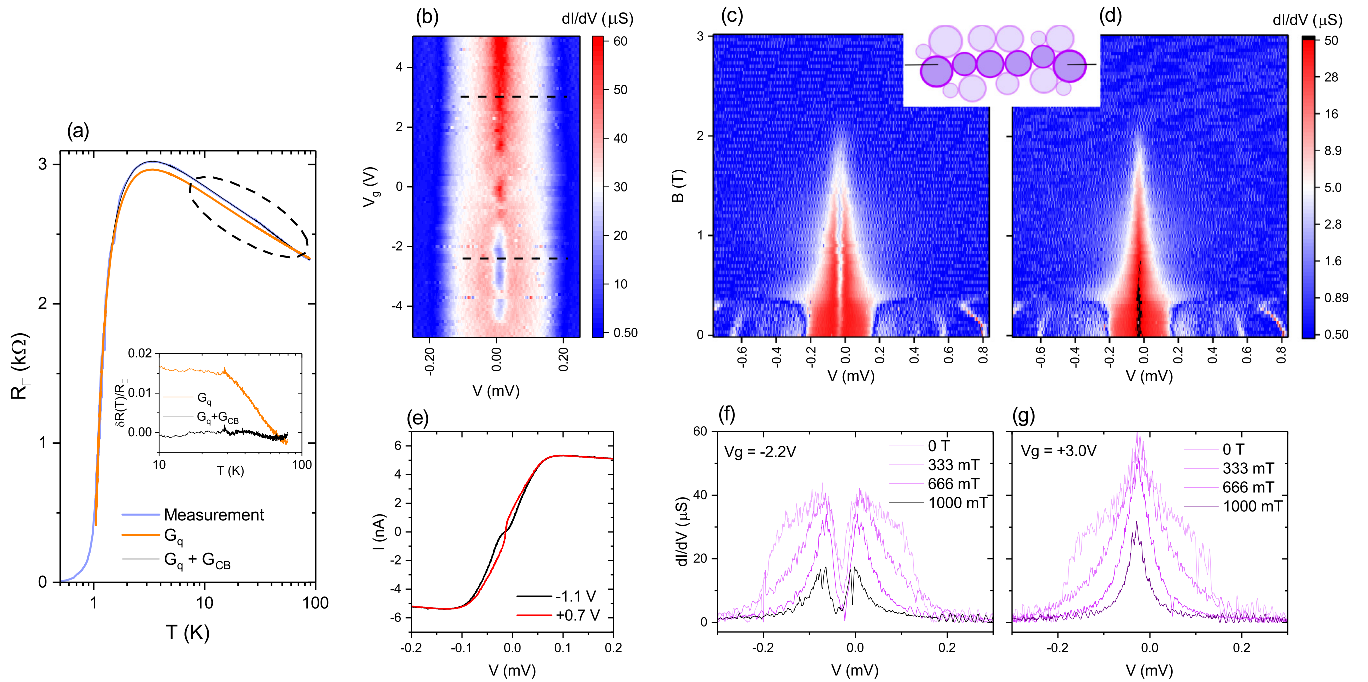

FIG. 3. Small blockade (device B). (a) Zero bias resistance as a function of temperature with fit to theory of quantum corrections for the conductivity. The inset shows the normalized residual resistance from the fits in the region highlighted by the dashed circle. (b) Differential conductance measured as a function of applied substrate back-gate voltage V_g. Dashed lines indicate the gate voltages in (c) and (d). (c),(d) Differential conductance measured at a gate voltage of −2.2 V and +3.0 V, respectively, versus applied perpendicular magnetic field. Vertical lines at low field and large bias are due to phase-slip centers in the inductive meanders. The inset shows a very simplified schematic sketch of the device. We attribute the small offset in bias voltage to our biasing circuitry. (e) Example of two IV curves showing the two extremes with a blockade voltage (black) and a superconducting branch (red). A resistance of 16 kΩ has been subtracted to highlight the superconducting branch. (f) and (g) Selected cross sections taken from (c) and (d), respectively.

showing no initial voltage blockade. The data is presented in Fig. 3. Despite the narrow width of meanders ($w_m = 100$ nm) they are still in the limit of 2D conductivity for all relevant temperatures. From the saturation in resistivity at high magnetic fields we estimate that the electronic temperature reaches ∼100 mK, corresponding to a maximum thermal length $L_{\rm th} = \sqrt{D\hbar/k_BT} = 52\,{\rm nm} < w_m$. Quantum corrections to the total conductivity G above T_c of a disordered 2D film is described by the Aronov-Altsuler (AA) electron-electron interaction, weak localization, and superconducting fluctuations from Maki-Thompson (MT), DOS and Aslamazov-Larkin (AL) corrections. We also add a contribution $G_{\rm CB}(T) = -c\ln{[gE_c/\max{(T,\Gamma)}]}$ from granularity and single electron charging effects of (some of) the grains [33,34], and the normal Drude term G_n. The total conductivity is given by (see Supplemental Material [29] for full details) [13]: $G = G_n + G_{\rm AA} + G_{\rm MT} + G_{\rm DOS} + G_{\rm AL} + G_{\rm CB} \equiv G_{\rm q} + G_{\rm CB}$.

The R(T) dependence of device B with fits to G is shown in Fig. 3(a). The broadened change in slope of the resistance at ≈32 K can be interpreted as originating from a few poorly connected grains with a distribution of sizes (in the otherwise homogeneous film) freezing out due to Coulomb blockade (CB). These poorly connected grains are located in the wider meanders; the nanowire itself is homogeneous and no blockade is seen in the current-voltage (IV) curves.

From the saturation of the CB term we extract an average grain level broadening $\Gamma/k_B = g\delta/k_B = 32$ K giving an average intergrain dimensionless conductance $g = G/(2e^2/h) = 2.4$. Taking the single grain charging energy from device A, $E_c/k_B = 23$ K, as a representation of the average grain charging energy we find an exceptionally good fit to $R(T)$ [Fig. 3(a)]. For comparison we also show the calculated resistance excluding the $G_{\rm CB}$ term. From this we conclude that the film is on average homogeneous with strongly connected grains with $b < b_{\rm crit}$, however, a smaller number of grains are weakly coupled which stochastically affects the transport characteristics of nanopatterned devices.

We now explore this device (B) in an applied magnetic and electric field. The response to a gate voltage, shown in Fig. 3(b), is much weaker than what is to be expected from a single grain dominating the transport (device A). For negative gate voltages a gap emerges of maximum size $V_c \sim 40\ \mu$V. The gate response occurs at voltages two orders of magnitude larger than for the SET-like devices.

Next, by fixing the gate voltage at −2.2 V and measuring V_c as a function of applied magnetic field [Figs. 3(c) and (f)] we observe that V_c is increasing as we approach $B_{c2\perp}$. Above $B_{c2\perp}$ V_c becomes negligibly small. On the contrary, for positive gate voltages we observe an increasing zero-bias conductance, shown in Figs. 3(d) and 3(g). IV curves for the two extremes are shown in Fig. 3(e) for comparison. This is reminiscent of a ‘critical current’ corresponding to ≈1 nA. This should be put in relation to the critical current of the 100 nm wide meanders which is $I_c \approx 5$ nA. Assuming the same critical current density throughout the whole device this translates to a nanowire width of about 20 nm, as expected.

This excess critical current is suppressed in an applied magnetic field [Figs. 3(d) and 3(g)]. If we further attribute the residual resistance below the critical current of the nanowire to contact/lead series resistance (∼16 kΩ) we find a resistance of the nanowire itself of 13.7 kΩ, corresponding to 4.6 $R_\square$, or a 100 nm long nanowire of width 22 nm. We note that the series resistance could not be due to phase diffusion as the junction capacitance required to sustain the observed supercurrent of 1 nA must be in excess of 80 fF ($E_c < E_J = \Phi_0 I_c/2\pi$), in which case residual resistance due to phase diffusion becomes negligible.

We also note that slowly repeating the measurement in Fig. 3(b) multiple times (not shown) yields the same global dependence. However, the smaller features vary in position and intensity between measurements. Charge relaxation on a time scale of several minutes is also observed, consistent with the behavior of charge traps in the substrate, or in the remaining hydrogen silsesquioxane (HSQ) resist, near the nanowire.

The weak gate dependence of devices B could be an indication of QPS interference, as the induced charge along the nanowire is expected to result in interference of QPS amplitudes, suppressing the phase-slip rate due to the Aharonov-Casher (AC) effect [24]. The relevant scale for charge localization deep in the phase-slip regime is on the order of $\xi = \sqrt{\xi_0 l} \approx 2$ nm, where l is the mean free path [35]. This length scale is consistent with the much weaker gate dependence, as compared to the charging of a granule (device A). We interpret these results as the emergence of a few stronger phase slip centers along the wire. The gate dependence arises due to one or more larger segments of the wire being enclosed by these stronger phase slip centers. This can be understood in analogy to the simplest such implementation: the charge quantum interference device [24]. The elementary building blocks, corresponding to sketch B in Fig. 1(c), would be a gateable grain (or cluster of well-connected grains) connected to the rest of the wire via two QPS junctions, being regions of enhanced phase slip rate. Due to the nontrivial gate dependence we are likely dealing with a more complicated geometry than what is schematically sketched in Fig. 1(c) and in the inset of Fig. 3(c).

If we assume that we are able to arrange complete destructive interference of QPS amplitudes ($V_c = 0$) using the gate, this situation should be the dual to a Josephson junction where the critical current is suppressed; no voltage gap develops since phase coherence is maintained, and the junction instead turns dissipative. In a high impedance environment ($E_s \gg E_L = \Phi_0^2/2N_\square L_{k,\square}$) charge is the well defined quantum variable. Suppressing the phase-slip rate is not sufficient to establish the required phase coherence to observe a 'critical current' branch. However, for an intermediate impedance, as in our case, both regimes would still be accessible for a QPS wire, which we argue is the case of device B.

Phase slip rate

From the measured critical voltage below B_{c2} we can calculate the phase-slip rate $E_s = 2eV_c/2\pi$, for devices B (and C, discussed below) which ranges between 3 and 17 GHz ($30 \div 220$ μV), on the same order as obtained in coherent measurements of QPS qubits [20–23], and in good agreement with the theoretical expectations for the phase-slip rate in short wires [20,21,36]

$$E_s = \Delta\sqrt{\frac{L}{\xi}\frac{R_{2q}}{R_\xi}}\exp\left(-a\frac{R_{2q}}{R_\xi}\right), \qquad (1)$$

where $a \approx 0.36$ for a diffusive conductor [37], and R_ξ is the normal state resistance of a wire segment of length ξ. We thus expect $E_s \approx 5$ GHz ≈ 60 μV for device B given the previously estimated wire dimensions. Charge control of the QPS rate allows us to tune the nanowire through the SIT via the AC effect.

The blockade in device B also fulfils an important criteria for attributing the blockade to QPS: $V_c < 2\Delta \approx 290$ μV. The relatively small blockade is an indication of a large kinetic capacitance due to quantum phase slips [14,38] $C_k = 2e/2\pi V_c = e^2/\pi^2 E_s = 0.1 \div 0.9$ fF, much larger than any achievable geometric capacitance of any part of the homogeneous device and between any grains.

D. Intermediate device

We now turn to device C (Fig. 4), showing a behavior very similar to that reported in Ref. [14]. There it was suggested that the peak in conductivity above $B_{c2\perp}$ is due to the order parameter inside grains persisting to magnetic fields much higher than those that suppress intergrain couplings, which allowed for good agreement between experiment and theory by a duality transformation applied to the theory of transport in over-damped small Josephson junctions [39]. Our data for two magnetic field orientations is shown in Figs. 4(a) and 4(b), respectively. A smeared voltage gap of $V_c \approx 200$ μV is seen at $B = 0$, and increasing the field reveals an oscillatory behavior of the gap persisting well above the suppression of the critical current, strikingly similar to Ref. [14]. We also note that these oscillations vary between cool downs from room temperature [(c.f. Fig. 4(e)], as would be expected from a bosonic SIT and spontaneously formed electronic inhomogeneity [40], and that they are perfectly symmetric with respect to field orientation: $V_c(+B) = V_c(-B)$. This particular device was only possible to gate to ±300 mV after which the gate dielectric started to leak, but only a very weak (<5%) variation in V_c was observed in this range (not shown), similar to device B.

While the zero field data for the two datasets in Figs. 4(a) and 4(b) are very similar, for even modest fields the blockade becomes much sharper for the perpendicular field orientation. This onset is consistent with the expected vortex entry field in the superinductor $B_\perp = \Phi_0\sqrt{2d/\pi w}/(2\pi\lambda_L\xi) \approx 30$ mT, and the effect can be attributed to quasiparticle trapping by vortex cores [41] cooling the nanowire. In Fig. 4(c) we compare two IV curves for the two field orientations where the applied field is such that the critical current of the meanders is suppressed to the same value. Interestingly even above B_{c2} the gap remains much sharper for the perpendicular field orientation, a behavior significantly different from the field-induced parity effects in insulating Josephson junction chains [42]. Similar behavior was instead seen in wider TiN [43] and InO films [44] which can be phenomenologically described by anisotropic orbital effects competing with the isotropic

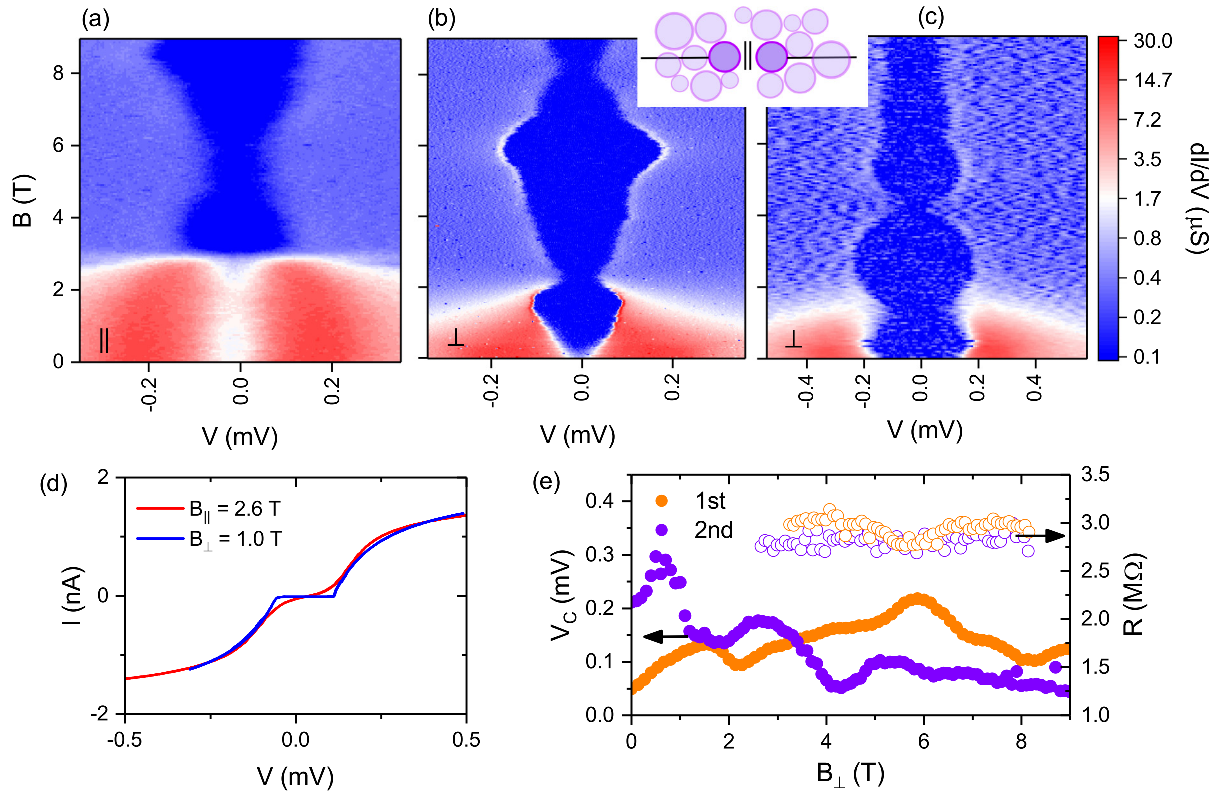

FIG. 4. Intermediate blockade (device C). (a) Differential conductance measured as a function of parallel magnetic field and (b) and (c) perpendicular field in two consecutive cool downs, respectively. The inset shows a very simplified sketch of the likely device geometry. (d) Comparison of IV curves for magnetic fields where critical currents of meanders have been suppressed equally. (e) Extracted blockade voltage V_c (solid markers) and normal state resistance (hollow markers) from the data in (b) (purple) and (c) (orange).

Zeeman effect, governing the percolation of superconductivity [45].

Peak in didv in the normal state and gap modulation

The peaks in $\partial I/\partial V$ at $V = \pm V_c$ remains above B_{c2}. The absence of SET-like behavior could indicate the presence of a single tunnel junction as opposed to QPS. The well established P(E) theory [46] describing tunnel junctions in high impedance environments fails to reproduce the peak in conductance at the gap edge under the assumption of a constant DOS in the normal state. The required nonlinear DOS at the Fermi level is expected from disordered superconductors even in the normal state near the SIT even well above T_c and B_{c2} [9,40,47], supporting the debated notion that superconducting fluctuations persist in grains well above B_{c2}. However, the smearing of the gap above $B_{c2\|}$ and a smaller zero bias resistance compared to $B_{c2\perp}$ could not be explained within this scenario alone. An onset of back bending of an IV curve above V_c could be a signature of the so-called Bloch nose due to coherent charge oscillations. However, such features could also be attributed to overheating due to weak electron-phonon coupling resulting in poor dissipation of the Joule heating in the resistive state [48,49]. These effects could not be directly distinguished in a typical IV trace, however, overheating is not expected to yield the observed gate and magnetic field dependence of V_c. In particular, the B modulation of the gap could be attributed to the isotropic Zeeman splitting of energy levels in the grains [33,50]. Their low and broadened DOS will thus vary in B, changing the conductivity of the nanowire, in analogy with an electrostatic gate. The difference in gap modulation between 4(b) and 4(c) could arise due to aging and/or the spontaneous formation of different percolation networks of superconducting islands, uncorrelated from the underlying metallurgical film morphology, in the different cool downs, separated by six months in time. This picture is also supported by the observed magnetoconductance of device A which shows a similar, but weaker, modulating behavior of the gap (see Supplemental Material [29]).

The absence of a strong gate effect would thus imply that in sample C we are most likely dealing with a single well-developed tunnel junction between the granular, but continuous leads, a statistically plausible scenario in a confined geometry, falling in-between devices A and B. The DOS in this system may still be subject to local superconducting fluctuations.

IV. CONCLUSIONS

To conclude, we have shown transport measurements on narrow TiN nanowires embedded in a high impedance superinductor environment. By studying the behavior both in magnetic field and as a function of applied gate voltages

we are able to identify nanowires exhibiting several regimes; both incoherent Coulomb blockade in single isolated grains in the film as well as new interesting physics in wires that appear to be much more homogeneous and show indications of coherent quantum phase slips controlled by electrostatic gate. Our work highlights the stochastic nature of these on average homogeneously disordered nanowires where isolated grains may be present that can influence device physics.

ACKNOWLEDGMENTS

We thank Y. Nazarov, A. V. Danilov, and I. Rungger for fruitful discussions, T. M. Klapwijk for providing the TiN films, and T. Hönigl-Decrinis for assistance with sample preparation. Samples were fabricated in the nanofabrication facilities of the department of microtechnology and nanoscience at Chalmers university and at Royal Holloway university of London. This work was supported by the UK Department of Business, Energy and Industrial Strategy (BEIS).

[1] J. T. Peltonen, P. C. J. J. Coumou, Z. H. Peng, T. M. Klapwijk, J. S. Tsai, and O. V. Astafiev, Sci. Rep. **8**, 10033 (2018).
[2] T. M. Hazard, A. Gyenis, A. DiPaolo, A. T. Asfaw, S. A. Lyon, A. Blais, and A. A. Houck, Phys. Rev. Lett. **122**, 010504 (2019).
[3] D. Niepce, J. Burnett, and J. Bylander, Phys. Rev. Applied **11**, 044014 (2019).
[4] J. S. Lehtinen, K. Zakharov, and K. Yu. Arutyunov, Phys. Rev. Lett. **109**, 187001 (2012).
[5] V. F. Gantmakher and V. T. Dolgopolov, Phys.-Usp. **53**, 1 (2010).
[6] M. V. Feigel'man and L. B. Ioffe, Phys. Rev. Lett. **120**, 037004 (2018).
[7] M. V. Feigel'man, L. B. Ioffe, V. E. Kravtsov, and E. Cuevas, Ann. Phys. **325**, 1390 (2010).
[8] B. Sacépé, C. Chapelier, T. I. Baturina, V. M. Vinokur, M. R. Baklanov, and M. Sanquer, Phys. Rev. Lett. **101**, 157006 (2008).
[9] B. Sacépé, C. Chapelier, T. I. Baturina, V. M. Vinokur, M. R. Baklanov, and M. Sanquer, Nat. Commun. **1**, 140 (2010).
[10] R. Córdoba, T. I. Baturina, J. Sesé, A. Yu. Mironov, J. M. De Teresa, M. R. Ibarra, D. A. Nasimov, A. K. Gutakovskii, A. V. Latyshev, I. Guillamón, H. Suderow, S. Vieira, M. R. Baklanov, J. J. Palacios, and V. M. Vinokur, Nat. Commun. **4**, 1437 (2013).
[11] S. V. Postolova, A. Yu. Mironov, and T. L. Baturina, JETP Lett. **100**, 635 (2014).
[12] E. F. C. Driessen, P. C. J. J. Coumou, R. R. Tromp, P. J. de Visser, and T. M. Klapwijk, Phys. Rev. Lett. **109**, 107003 (2012).
[13] T. I. Baturina, S. V. Postolova, A. Yu. Mironov, A. Glatz, M. R. Baklanov, and V. M. Vinokur, Eur. Phys. Lett. **97**, 17012 (2012).
[14] I. Schneider, K. Kronfeldner, T. I. Baturina, and C. Strunk, Phys. Rev. B **99**, 094522 (2019).
[15] N. G. N. Constantino, M. S. Anwar, O. W. Kennedy, M. Dang, P. A. Warburton, and J. C. Fenton, Nanomaterials **8**, 442 (2018).
[16] A. Yu. Mironov, S. V. Postolova, and D. A. Nasimov, JETP Lett. **104**, 766 (2016).
[17] T. T. Hongisto and A. B. Zorin, Phys. Rev. Lett. **108**, 097001 (2012).
[18] C. H. Webster, J. C. Fenton, T. T. Hongisto, S. P. Giblin, A. B. Zorin, and P. A. Warburton, Phys. Rev. B **87**, 144510 (2013).
[19] W. Guichard and F. W. J. Hekking, Phys. Rev. B **81**, 064508 (2010).
[20] O. V. Astafiev, L. B. Ioffe, S. Kafanov, Yu. A. Pashkin, K. Yu. Arutyonov, D. Shahar, O. Cohen, and J. S. Tsai, Nature (London) **484**, 355 (2012).
[21] J. T. Peltonen, O. V. Astafiev, Yu. P. Korneeva, B. M. Voronov, A. A. Korneev, I. M. Charaev, A. V. Semenov, G. N. Golt'sman, L. B. Ioffe, T. M. Klapwijk, and J. S. Tsai, Phys Rev. B **88**, 220506 (2013).
[22] J. T. Peltonen, Z. H. Peng, Yu. P. Korneeva, B. M. Voronov, A. A. Korneev, A. V. Semenov, G. N. Gol'tsman, J. S. Tsai, and O. V. Astafiev, Phys. Rev. B **94**, 180508 (2016).
[23] J. T. Peltonen, P. C. J. J. Coumou, T. M. Klapwijk, J. S. Tsai, and O. V. Astafiev (unpublished).
[24] S. E. de Graaf, S. T. Skacel, T. Hönigl-Decrinis, R. Shaikhaidarov, H. Rotzinger, S. Linzen, M. Ziegler, U. Hübner, H.-G. Meyer, V. Antonov, E. Il'ichev, A. V. Ustinov, A. Ya. Tzalenchuk, and O. V. Astafiev, Nat. Phys. **14**, 590 (2018).
[25] N. A. Masluk, I. M. Pop, A. Kamal, Z. K. Minev, and M. H. Devoret, Phys. Rev. Lett. **109**, 137002 (2012).
[26] W. Zhang, K. Kalashnikov, W.-S. Lu, P. Kamenov, T. Di Napoli, and M. E. Gershenson, Phys. Rev. Applied **11**, 011003 (2019).
[27] A. Di Marco, F. W. J. Hekking, and G. Rastelli, Phys. Rev. B **91**, 184512 (2015).
[28] P. C. J. J. Coumou, E. F. C. Driessen, J. Bueno, C. Chapelier, and T. M. Klapwijk, Phys. Rev. B **88**, 180505(R) (2013).
[29] See Supplemental Material at http://link.aps.org/supplemental/10.1103/PhysRevB.99.205115 for further details on samples, methods and material properties.
[30] A. Kardakova, M. Finkel, D. Morozov, V. Kovalyuk, P. An, C. Dunscombe, M. Tarkhov, P. Mauskopf, T. M. Klapwijk, and G. Goltsman, Appl. Phys. Lett. **103**, 252602 (2013).
[31] R. A. Parker, Phys. Rev. **124**, 1719 (1961).
[32] S. Logothetidis, E. I. Meletis, G. Stergioudis, and A. A. Adjaottor, Thin Solid Films **338**, 304 (1999).
[33] I. S. Beloborodov, A. V. Lopatin, V. M. Vinokur, and K. B. Efetov, Rev. Mod. Phys. **79**, 469 (2007).
[34] K. B. Efetov and A. Tschersich, Phys. Rev. B **67**, 174205 (2003).
[35] J. E. Mooij, New J. Phys. **17**, 033006 (2013).
[36] K. Yu. Arutyunov, D. S. Golubev, and A. D. Zaikin, Phys. Rep. **464**, 1 (2008).
[37] M. Vanevic and Y. V. Nazarov, Phys. Rev. Lett. **108**, 187002 (2012).
[38] J. E. Mooij, and Yu. V. Nazarov, Nat. Phys. **2**, 169 (2006).
[39] Y. M. Ivanchenko and L. A. Zil'berman, Zh. Eksp. Teor. Fiz. **55**, 2395 (1968) [Sov. Phys. JETP **28**, 1272 (1969)].
[40] Y. Dubi, Y. Meir, and Y. Avishai, Nature (London) **449**, 876 (2007).

[41] M. Taupin, I. M. Khaymovich, M. Meschke, A. S. Mel'nikov, and J. P. Pekola, Nat. Commun. **7**, 10977 (2016).
[42] T. Duty, K. Cedergren, S. Kafanov, R. Ackroyd, and J. H. Cole, arXiv:1808.08552.
[43] D. Kalok, Ph.D. thesis, University of Regensburg, 2012.
[44] A. Johansson, I. Shammass, N. Stander, E. Peled, G. Sambandamurthy, and D. Shahar, Solid State Commun. **151**, 743 (2011).
[45] E. Porat and Y. Meir, Phys. Rev. B. **92**, 024509 (2015).
[46] G.-L. Ingold and Yu. V. Nazarov in *Single Charge Tunneling*, edited by H. Grabert and M. H. Devoret, NATO ASI Series B Vol. 294 (Plenum Press, New York, 1992), pp. 21–107.
[47] T. Dubouchet, B. Sacépé, J. Seidemann, D. Shahar, M. Sanquer, and C. Chapelier, Nat. Phys. **15**, 233 (2019).
[48] M. Ovadia, B. Sacépé, and D. Sahar, Phys. Rev. Lett. **102**, 176802 (2009).
[49] B. L. Altshuler, V. E. Kravtsov, I. V. Lerner, and I. L. Aleiner, Phys. Rev. Lett. **102**, 176803 (2009).
[50] B. Dong and N. J. M. Horing, and H. L. Cui, Phys. Rev. B **72**, 165326 (2005).